

Textured 3D Regenerative Morphing with 3D Diffusion Prior

SONGLIN YANG, S-Lab, Nanyang Technological University, Singapore

YUSHI LAN, S-Lab, Nanyang Technological University, Singapore

HONGHUA CHEN, S-Lab, Nanyang Technological University, Singapore

XINGANG PAN, S-Lab, Nanyang Technological University, Singapore

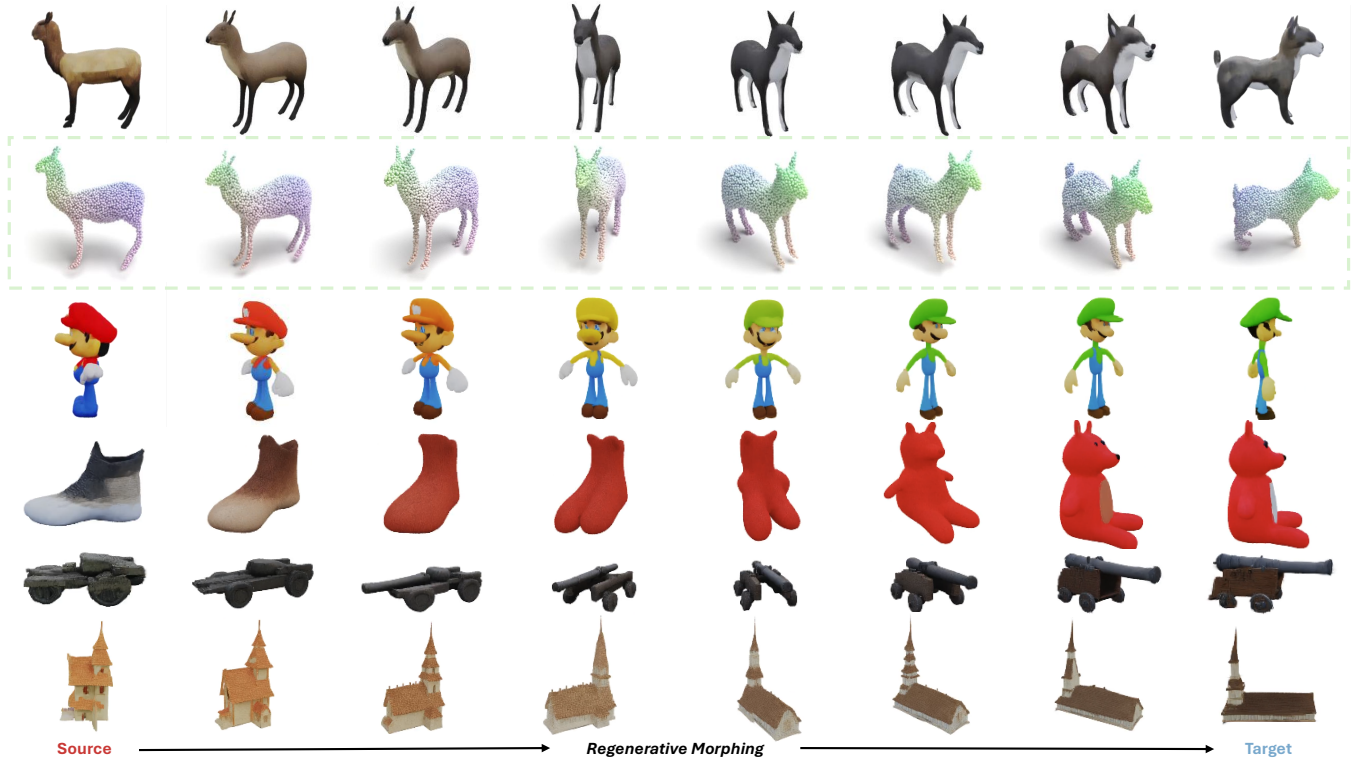


Fig. 1. The textured 3D morphing sequences regenerated using our method with 3D diffusion prior. Our method requires no category-specific alignment data for model training and no labor-intensive preprocessing for explicit correspondence, enabling smooth and plausible morphing across diverse cross-category 3D object pairs. **More video results can be found [here](#).**

Textured 3D morphing creates *smooth* and *plausible* interpolation sequences between two 3D objects, focusing on transitions in both shape and texture. This is important for creative applications like visual effects in filmmaking. Previous methods rely on establishing point-to-point correspondences and determining smooth deformation trajectories, which inherently restrict them to shape-only morphing on untextured, topologically aligned datasets. This restriction leads to labor-intensive preprocessing and poor generalization. To overcome these challenges, we propose a method for 3D regenerative morphing using a 3D diffusion prior. Unlike previous methods that depend on explicit correspondences and deformations, our method eliminates the additional need for obtaining correspondence and uses the 3D diffusion prior to generate morphing. Specifically, we introduce a 3D diffusion model and interpolate the source and target information at three levels: initial

noise, model parameters, and condition features. We then explore an **Attention Fusion** strategy to generate more smooth morphing sequences. To further improve the plausibility of semantic interpolation and the generated 3D surfaces, we propose two strategies: **(a) Token Reordering**, where we match approximate tokens based on semantic analysis to guide implicit correspondences in the denoising process of the diffusion model, and **(b) Low-Frequency Enhancement**, where we enhance low-frequency signals in the tokens to improve the quality of generated surfaces. Experimental results show that our method achieves superior smoothness and plausibility in 3D morphing across diverse cross-category object pairs, offering a novel regenerative method for 3D morphing with textured representations.

CCS Concepts: • **Computing methodologies** → **Computer graphics; Appearance and texture representations; Shape analysis.**

Authors' Contact Information: Songlin Yang, S-Lab, Nanyang Technological University, Singapore, songlin.yang@ntu.edu.sg; Yushi Lan, S-Lab, Nanyang Technological University, Singapore, yushi001@e.ntu.edu.sg; Honghua Chen, S-Lab, Nanyang Technological University, Singapore, honghua.chen@ntu.edu.sg; Xingang Pan, S-Lab, Nanyang Technological University, Singapore, xingang.pan@ntu.edu.sg.

Additional Key Words and Phrases: Textured 3D Morphing, 3D Generation, 3D Diffusion Models

1 Introduction

Morphing [Lin et al. 2024] generates an interpolation sequence between a source and a target, requiring smooth and plausible transitions. This fundamental technique is crucial for creative applications like visual effects in film and media. Depending on the data type, morphing is categorized into image morphing [Shechtman et al. 2010; Zhang et al. 2024] and 3D morphing [Geng et al. 2024; Kim et al. 2024; Tsai et al. 2022]. Compared to image morphing, 3D morphing aligns more naturally with visual effects production, where objects and transformations inherently operate in 3D space. However, 3D morphing is more challenging, requiring the interpolation of 3D objects holistically (i.e., image morphing can be viewed as a special case of 3D morphing from a specific viewpoint). Our work addresses the task of textured 3D morphing, which generates a sequence for two textured 3D representations, aiming for smooth and plausible transitions in shape and texture, as shown in Fig. 1.

Previous 3D morphing methods mainly focused on morphing shapes, which can be summarized in two steps: *first*, establishing correspondence [Deng et al. 2023] between the 3D representations of the source and target objects, and *second*, determining smooth and plausible deformation trajectories between corresponding 3D points [Eisenberger et al. 2021]. Following these steps, previous methods blend the two 3D representations with respective weights to obtain a sequence of interpolated 3D representations.

Due to the scarcity of topologically aligned and textured 3D datasets, previous 3D morphing methods have mainly focused on in-domain untextured datasets, such as FAUST [Bogo et al. 2014] (human shapes) and Shrec’20 [Dyke et al. 2020] (quadruped animals). As a result, these methods are limited to **shape-only morphing** and face two key **generalization** challenges: (a) *Labor-Intensive Preprocessing*: Morphing new in-domain 3D data with these methods [Eisenberger et al. 2021; Zhan et al. 2024] requires domain-specific alignment with the training datasets through tedious registration [Sun et al. 2024] and matching [Zhu et al. 2024] steps. (b) *Limited Morphing Capacity*: The methods [Aydnlılar and Sahillioğlu 2021; Eisenberger et al. 2021; Vyas et al. 2021; Zhan et al. 2024] suffer from limited object diversity and small datasets, leading to ambiguous and implausible interpolations.

The limitations of previous methods inspire us to consider two critical questions: (a) *Is explicit point-to-point correspondence truly necessary?* (b) *Can we enhance the generalization capability of textured 3D morphing via a generic generative prior?*

For **correspondence**, obtaining dense correspondences between textured 3D representations across categories remains underexplored [Zhu et al. 2024] despite being foundational to previous methods, while explicit constraints can instead limit the creativity of morphing. Therefore, a promising method is using labor-saving implicit correspondences [Lan et al. 2022; Yang et al. 2024] to guide the morphing. For instance, morphing could be formulated as an optimization problem, allowing correspondences to emerge automatically [Tsai et al. 2022]. Alternatively, attention mechanisms in generative models could enable automatic alignment during object blending [He et al. 2024; Shen et al. 2024; Zhang et al. 2024].

For **generative priors**, recent advancements in diffusion-based generation models offer two strategies for 3D morphing: using 3D

diffusion models directly [Chen et al. 2024a; Lan et al. 2025b; Xiang et al. 2024], or enhancing 2D models with 3D priors. However, those hybrid 2D-3D methods [Haque et al. 2023; Kim et al. 2024; Poole et al. 2022; Rombach et al. 2022] face significant challenges: 2D models lack a holistic 3D knowledge, and optimizing the 2D-3D mapping is difficult, with no guarantee that the morphing process will maintain 3D consistency across viewpoints. Therefore, directly using a 3D diffusion model to regenerate the interpolated 3D representations (i.e., regenerative morphing) enables authentic 3D morphing and has the potential to be scaled up by using a more state-of-the-art 3D generation model.

Building on the above analysis, we adopt a generic 3D diffusion prior that leverages its implicit correspondence and 3D generation capabilities to blend source and target information, enabling the regeneration of interpolated textured 3D representations.

Specifically, we first introduce a 3D diffusion model [Lan et al. 2025b] and interpolate the information from the source and target at three levels: initial noises, model parameters, and condition features. The 3D representation for each interpolation is then regenerated using the 3D generation model. To improve the 3D diffusion model’s ability to generate smooth morphing sequences, we explore an **Attention Fusion** strategy. However, fusing different information weakened the model’s denoising capability, and aggressively applying Attention Fusion to all denoising steps for smoother morphing resulted in implausible outcomes. Therefore, to improve the plausibility of semantic interpolation and the generated 3D surfaces, we propose two strategies: (a) **Token Reordering**: After semantic analysis, we identify semantic correspondences in diffusion tokens and propose matching approximate tokens before attention computation to better guide implicit correspondences in the diffusion space. (b) **Low-Frequency Enhancement**: Frequency-domain analysis reveals that boosting low-frequency signals improves the surface quality of the 3D diffusion model. Thus, we enhance low-frequency signals at key time steps to preserve the model’s ability to generate 3D surfaces.

Our contributions can be summarized as follows: (a) To the best of our knowledge, we are the first to use a generic 3D diffusion prior for morphing textured 3D representations, enabling 3D morphing without explicit correspondences. (b) We analyze the merging of source and target information during morphing with a 3D diffusion prior from semantic and frequency perspectives, proposing Token Reordering and Low-Frequency Enhancement to improve smoothness and plausibility. (c) Extensive experimental results demonstrate that our method achieves superior smoothness and plausibility in performing 3D morphing across diverse cross-category object pairs.

2 Related Work

2.1 3D Morphing

Previous 3D morphing methods focus on shape-only correspondence [Tam et al. 2012], and realize 3D morphing through interpolation or deformation between corresponding 3D primitives (e.g., points, vertices, and faces). They can be divided into (a) *Axiomatic Methods*: They tend to rely on sparse landmarks [Edelstein et al. 2019; Kim et al. 2011] or use functional maps [Ovsjanikov et al. 2012] to address under-constrained mapping spaces, such as Map-Tree [Ren et al. 2020] and SmoothShells [Eisenberger et al. 2020].

Energy-minimizing functions [Sorkine and Alexa 2007; Sorkine et al. 2004] and skinning methods [Fulton et al. 2019; Jacobson et al. 2014] enable deformation control, while optimal transportation [Solomon et al. 2015; Tsai et al. 2022] approximates shape correspondence. *(b) Learning-Based Methods:* This category of methods can be categorized into introducing other generative priors and using aligned data. SATR [Abdelreheem et al. 2023] introduces the semantic labels from multi-view images. NSSM [Morreale et al. 2024] uses Dinov2 [Oquab et al. 2023] for sparse landmarks and SRIF [Sun et al. 2024] introduces large vision models [Zhang et al. 2024] for semantic shape registration and morphing. A recent class of works leverages text prompts as user inputs for driving a deformation towards an arbitrary textual prompt [Gao et al. 2023; Michel et al. 2022; Mohammad Khalid et al. 2022], but CLIP [Radford et al. 2021] objective lacks a full understanding of object details. For data prior, category-specific training [Yumer et al. 2015] on a topology-aligned dataset such as NeuroMorph [Eisenberger et al. 2021] is also prevailing in learning-based 3D shape analysis.

These methods focus on shape-only morphing or rely on rigging annotations, requiring extra effort due to 2D-3D mismatches. In contrast, our work enables textured 3D morphing without learning correspondence or deformation, using a 3D diffusion model to regenerate interpolated representations, addressing prior challenges and offering a new direction for 3D morphing research.

2.2 Image Morphing

Image morphing is a long-standing challenge in computer vision and graphics [Aloraibi 2023; Wolberg 1998; Zope and Zope 2017]. Traditional methods [Beier and Neely 2023; Bhatt 2011; Darabi et al. 2012; Liao et al. 2014; Shechtman et al. 2010] use feature-based warping and blending to create smooth transitions but struggle to generate new content, often leading to artifacts. Data-driven methods [Averbuch-Elor et al. 2016; Fish et al. 2020] leverage large single-class datasets to achieve smoother results but are limited in cross-domain or personalized applications due to their reliance on specific data. The methods like DiffMorpher [Zhang et al. 2024] and AID [He et al. 2024] address this by utilizing pre-trained diffusion models on diverse datasets, enabling flexible morphing across a wide range of object categories. *Inputting multi-view images to image morphing methods enables 3D-aware morphing.*

2.3 3D Diffusion Model

Generative 3D priors fall into two types: native 3D diffusion models and 3D-aware diffusion models. Due to the scarcity of 3D data, methods leveraging 2D priors to generate 3D or multi-view content have been proposed. For instance, Score Distillation Sampling [Poole et al. 2022] distills 3D information from a 2D diffusion model. 3D-aware generation can be divided into two steps: multi-view image generation [Shi et al. 2023] followed by feed-forward 3D reconstruction [Xu et al. 2024]. However, these methods inherently lack a 3D latent space. To address this, native 3D diffusion models [Lan et al. 2025a; Vahdat et al. 2022; Zhang et al. 2023] that encode and learn 3D representations have been introduced. These models typically consist of two steps: training a VAE to encode 3D data and training a diffusion model based on corresponding latent codes. We use Gaussian Anything [Lan et al. 2025b] as the 3D diffusion prior, encoding 3D information in a point cloud latent space.

3 Method

The pipeline for 3D regenerative morphing based on the 3D diffusion prior, as shown in Fig.2, consists of three main steps: **Basic Interpolation**, where essential information is interpolated (Sec.3.2); **Smoothness Improvement**, achieved through an Attention Fusion mechanism (Sec.3.3); and **Plausibility Improvement**, which involves two strategies, Token Reordering (Sec.3.4) and Low-Frequency Enhancement (Sec. 3.5).

3.1 Preliminary

3.1.1 3D Diffusion Model. We select Gaussian Anything [Lan et al. 2025b] as our 3D diffusion prior, a two-stage native 3D diffusion model with a structured latent representation (i.e., point cloud) and the DiT [Peebles and Xie 2023] backbone. It consists of a geometry generation model ϵ_G and a texture generation model ϵ_T . In the first stage, the model ϵ_G takes a Gaussian initial noise \mathbf{z}_G and textual conditioning information \mathbf{c} as inputs, to generate a structured point cloud representation $\mathbf{x}_{point-cloud} = \epsilon_G(\mathbf{z}_G, \mathbf{c})$. In the second stage, $\mathbf{x}_{point-cloud}$ is added to a Gaussian initial noise \mathbf{z}_T , and the resulting variable is denoised by ϵ_T with condition \mathbf{c} to obtain the final texture feature $\mathbf{x}_{feature} = \epsilon_T(\mathbf{x}_{point-cloud} + \mathbf{z}_T, \mathbf{c})$. Finally, $\mathbf{x}_{point-cloud}$ and $\mathbf{x}_{feature}$ are fed into a pre-trained decoder \mathcal{D} to produce the final 3D Gaussian representation $\mathbf{x}_{3D} = \mathcal{D}(\mathbf{x}_{point-cloud}, \mathbf{x}_{feature})$, which can be rendered as multi-view images. We denote the token sequences processed between DiT blocks as $\{h_j\}_{j=1}^M$, where M is the length of token sequence.

3.1.2 Attention. The attention [Vaswani 2017] mechanism is an important component for the current text-driven diffusion models [Chen et al. 2024a; Peebles and Xie 2023; Rombach et al. 2022; Saharia et al. 2022; Xiang et al. 2024], especially cross-attention and self-attention. Given a latent variable $z \in \mathbb{R}^{d_z}$, a text condition $c \in \mathbb{R}^{d_c}$, and the attention layer with matrices $W_Q \in \mathbb{R}^{d_z \times d_q}$, $W_K \in \mathbb{R}^{d_c \times d_k}$, and $W_V \in \mathbb{R}^{d_z \times d_v}$, the cross-attention is computed as:

$$A(z, c) = \text{Attn}(Q, K, V) = \text{softmax}\left(\frac{QK^T}{\sqrt{d_k}}\right)V, \quad (1)$$

where $Q = W_Q^T z$, $K = W_K^T c$, $V = W_V^T c$. Self-attention is a special case of cross-attention and can be computed with $A(z, z)$.

3.2 Basic Interpolation

3.2.1 Implementation. The basic interpolation has three levels, with source and target weights given by $(1 - \alpha)$ and α , respectively, where $\alpha = 0$ generates the source \mathbf{x}_{3D}^{src} , and $\alpha = 1$ generates the target \mathbf{x}_{3D}^{tgt} .

(a) Initial Noises: The textured 3D representations \mathbf{x}_{3D}^{src} and \mathbf{x}_{3D}^{tgt} are inverted via diffusion inversion [Lipman et al. 2022] to obtain their respective input noises, $[\mathbf{z}_T^{src}, \mathbf{z}_G^{src}]$ and $[\mathbf{z}_T^{tgt}, \mathbf{z}_G^{tgt}]$. To ensure Gaussian noise properties are preserved, spherical linear interpolation [Samuel et al. 2024] is applied to these noises to generate the interpolated noises, $[\mathbf{z}_T^\alpha, \mathbf{z}_G^\alpha]$.

(b) Model Parameters: Given \mathbf{x}_{3D}^{src} and \mathbf{x}_{3D}^{tgt} , we fine-tune the model using LoRA (Low-Rank Adaptation) [Hu et al. 2021] to obtain two sets of LoRA parameters. These parameters are then linearly interpolated and fused to obtain the morphing models ϵ_G^α and ϵ_T^α .

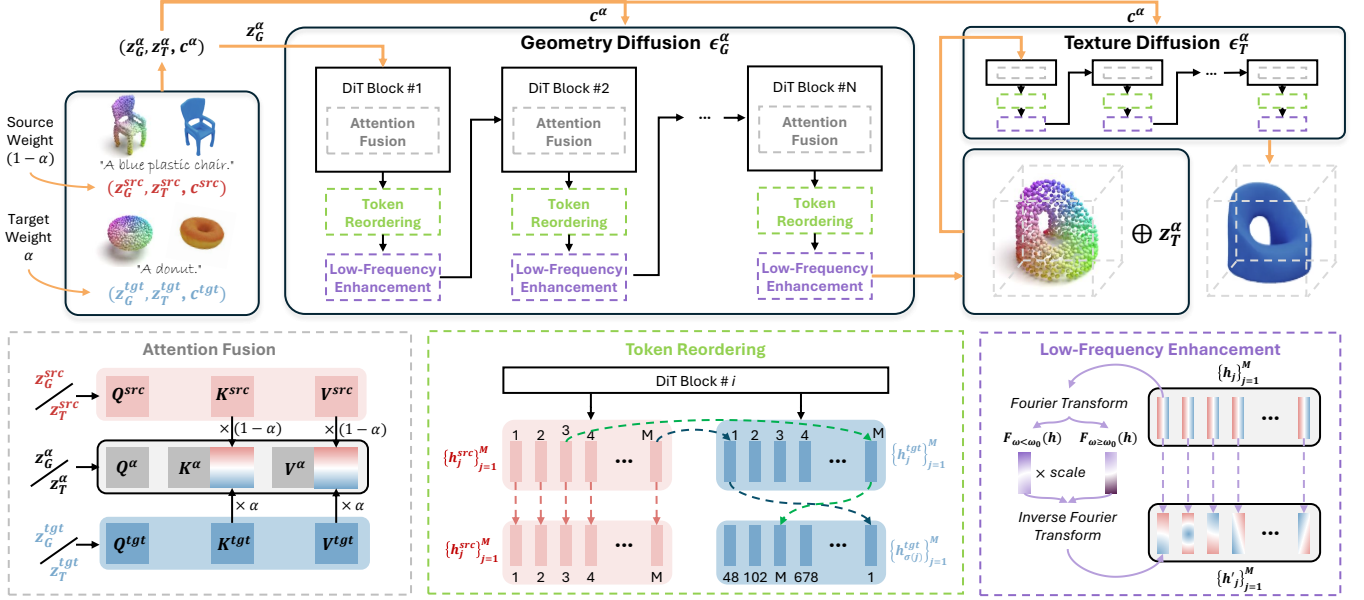


Fig. 2. The framework of our method. The 3D diffusion prior is a two-stage (geometry & texture) generation model. Beyond basic interpolation, Attention Fusion is explored to improve smoothness, while Token Reordering and Low-Frequency Enhancement are proposed to improve plausibility.

(c) *Condition Features*: To enhance semantic consistency, the text prompts of the source and target 3D representations are encoded via a CLIP [Radford et al. 2021] encoder into c^{src} and c^{tgt} , which are linearly interpolated to produce c^α .

3.2.2 *Problems*. Basic interpolation realizes the blending of basic information, but there are still the following problems:

(a) *Abrupt Changes (Smoothness)*: Nonlinear multi-step denoising in diffusion models introduces variability in noise-to-data mapping, while the CLIP encoder’s space lacks guaranteed semantic smoothness, leading to abrupt changes (yellow-highlighted part in Fig. 7).

(b) *Artifacts (Plausibility)*: Misalignment between conditioning and diffusion spaces disrupts learned mappings, causing artifacts like structure collapse or degraded surface quality (red and yellow-highlighted parts in Fig. 7).

To address these, we investigate **Attention Fusion** (Sec. 3.3) for smoothness and **Token Reordering** (Sec. 3.4) with **Low-Frequency Enhancement** (Sec. 3.5) for plausibility.

3.3 Attention Fusion

The fusion of attention has been proven effective in improving morphing smoothness in 2D diffusion-based image morphing. However, DiffMorpher [Zhang et al. 2024] only explored self-attention interpolation and did not consider the smoothness of semantic features in conditioning. AID [He et al. 2024] did not address the differences between the original and LoRA models, neglecting conditioning feature interpolation with accurate inversion. Our method combines self-attention and cross-attention fusion, using unified attention features from fine-tuned models to enhance smoothness while ensuring plausible generation.

Specifically, as shown in Fig. 2, we first feed z^{src} , z^{tgt} , and z^α into blocks of the morphing model ϵ^α to obtain three sets of $(Q^{src},$

K^{src}, V^{src}), $(Q^{tgt}, K^{tgt}, V^{tgt})$, and $(Q^\alpha, K^\alpha, V^\alpha)$. Then, based on Eq. (1), denoting concatenation as $[\cdot, \cdot]$, we obtain the fused attention by:

$$\begin{aligned} \text{Fused-Attn}(Q^\alpha, K^\alpha, V^\alpha) = \\ \text{Attn}\left(Q^\alpha, [(1-\alpha)K^{src} + \alpha K^{tgt}, K^\alpha], [(1-\alpha)V^{src} + \alpha V^{tgt}, V^\alpha]\right). \end{aligned} \quad (2)$$

Constraining all attention calculations to the same model helps mitigate the quality degradation caused by attention fusion. However, applying attention fusion across different time steps improves smoothness only to a point, beyond which plausibility declines, leading to structural collapse and surface issues (See Fig. 7). *This emphasizes the need to balance smoothness with plausibility.*

3.4 Token Reordering

3.4.1 *Motivation*. 3D objects are tokenized into sequences $\{h_j\}_{j=1}^M$, with each token h_j representing a 3D point. The DiT block’s attention modules and Attention Fusion guide the blending of source and target tokens using implicit correspondence during inference. However, relying solely on such implicit correspondence of attention mechanism to match the points in different 3D objects may lead the model to make semantically implausible connections (e.g., combining a chair leg with donut frosting). This vanilla application of the diffusion prior does not fully leverage its potential. Works like DIFT [Tang et al. 2023] show that 2D diffusion features/tokens can represent semantics [Hedlin et al. 2024; Yu et al. 2024; Zhang et al. 2025]. Similarly, we believe 3D diffusion features also capture 3D correspondences within the same object category and semantic correspondence across different object categories (e.g., the eyes of a dog and the eyes of a monkey). Therefore, *why not pair points with similar semantics first, and then interpolate within this semantically plausible space?*

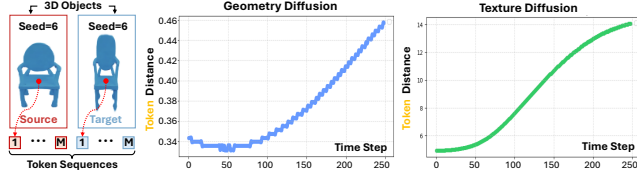


Fig. 3. The token distances between tokens at the same position in the sequence. A 3D representation is scaled to generate a perfectly aligned version with the same random seeds, ensuring tokens at the identical sequence positions are semantically aligned. During denoising, the semantic distance between tokens at the identical positions increases.

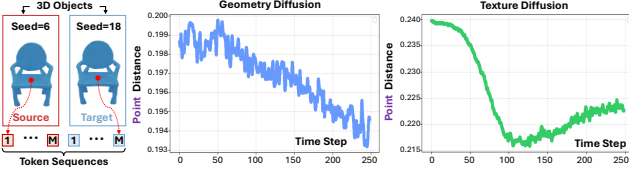


Fig. 4. The point distances between token-distance-closest points. Different random seeds are used to generate varied initial noises, meaning tokens at the identical sequence positions do not correspond to the same 3D points. By extracting the two closest tokens and their corresponding points in the final point cloud, we computed the 3D distance between the paired points.

3.4.2 Experimental Analysis. To validate our motivation, we tested the semantic correspondence of tokens on aligned data.

(a) *Problems of Vanilla Attention Fusion.* The Fig. 3 indicates that semantic alignment is lost during denoising, but vanilla Attention Fusion forcibly links these position-aligned tokens, which burdens the model and causes artifacts (See Fig. 7, third row).

(b) *Existence of Semantic Correspondence.* As shown in Fig. 4, the distance between points based on geometry token distance decreases with increasing time steps, indicating strengthened semantic correspondence. Conversely, the distance based on texture token distance first decreases and then increases, suggesting that the denoising process initially promotes semantic alignment, but later shifts towards learning texture details. This aligns with findings in 2D diffusion research [Yu et al. 2024]. Thus, by considering both geometry and texture denoising characteristics, we reorder tokens in the intermediate stages to better guide implicit correspondence for morphing.

3.4.3 Implementation. Based on these observations, we reorder the token sequences before passing the output of the i -th block to the $(i+1)$ -th block, where $i \in \{1, 2, \dots, N\}$ and N is the total number of blocks in the diffusion model. As shown in Fig. 2, we reorder the source and target token sequences $\{h_j^{\text{src}}\}_{j=1}^M, \{h_j^{\text{tgt}}\}_{j=1}^M$ such that tokens with similar distances align at the same index, as follows:

$$\text{minimize} \sum_{j=1}^M \|h_j^{\text{src}} - h_{\sigma(j)}^{\text{tgt}}\|, \quad (3)$$

where M is the number of tokens, and $\sigma(j)$ denotes the index of the element in the target sequence that best corresponds to the j -th element in the source sequence. To further refine the generation, we set different reordering strategies depending on α : For $\alpha \in [0, 0.5)$, the target token sequence is reordered based on the source token sequence. For $\alpha \in [0.5, 1]$, the source token sequence is reordered based on the target token sequence.

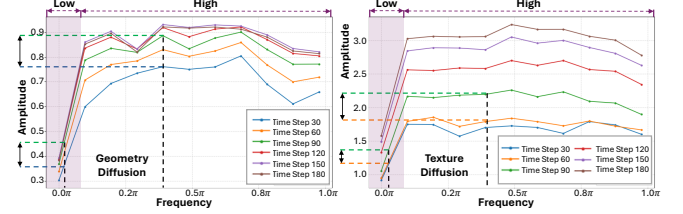


Fig. 5. The changes of high and low frequency signals in the diffusion model during the denoising process. Visualizing signal amplitudes at different time steps reveals that low-frequency noise varies less than high-frequency noise, with smaller gaps across denoising time steps.

3.5 Low-Frequency Enhancement

3.5.1 Motivation. Due to the additional attention fusion operations, the misalignment between the condition space and the diffusion space is exacerbated. Excessive attention fusion at later time steps significantly degrades the model’s denoising capability, with the deterioration becoming more pronounced as the time step increases (See Fig. 7, from the 4th to the 5th row). This raises the question: *what part of the 3D diffusion model is influenced by the morphing operations, leading to this decline in performance?*

3.5.2 Experimental Analysis. The deterioration problem is analyzed in the frequency domain to address the significant visual differences between 3D objects, as shown in Fig. 5. In 3D generation, low-frequency noise controls the overall layout, while high-frequency noise governs surface details. Excessive amplification of high-frequency components during denoising can interfere with the low-frequency components, degrading overall quality. Therefore, enhancing low-frequency signals during denoising is crucial to prevent the model from overemphasizing high-frequency noise, thus improving the quality of 3D surface generation. Similar patterns appear in 2D diffusion studies [Si et al. 2024; Wu et al. 2025], with low frequencies tied to image layout and high frequencies to details.

3.5.3 Implementation. To address this, as shown in Fig. 2, we propose to enhance the low-frequency signal when generating the 3D interpolations. Specifically, the process is defined as:

$$F(h) = \text{FFT}(h), \quad (4)$$

$$F'_{\omega < \omega_0}(h) = F_{\omega < \omega_0}(h) \odot \text{scale}, \quad (5)$$

$$h' = \text{IFFT}([F'_{\omega < \omega_0}(h), F_{\omega \geq \omega_0}(h)]), \quad (6)$$

where h represents the tokens, $F(h)$ their Fourier features, and h' the enhanced tokens, ω and ω_0 denote Fourier frequencies and the threshold, with $\omega < \omega_0$ indicating low-frequency components. The scale is the enhancement coefficient, and $\text{FFT}(\cdot)$ and $\text{IFFT}(\cdot)$ are the Fourier transform and inverse Fourier transform.

4 Experiments

4.1 Implementation Details

4.1.1 3D Generation Model. The 3D diffusion prior [Lan et al. 2025b] is trained on the G-Objaverse [Deitke et al. 2023] dataset. Its geometry and texture diffusion models are based on the DiT architecture [Chen et al. 2024b], which consists of 24 layers, 16 attention heads, and a 1024-dimensional hidden space. The sparse point cloud

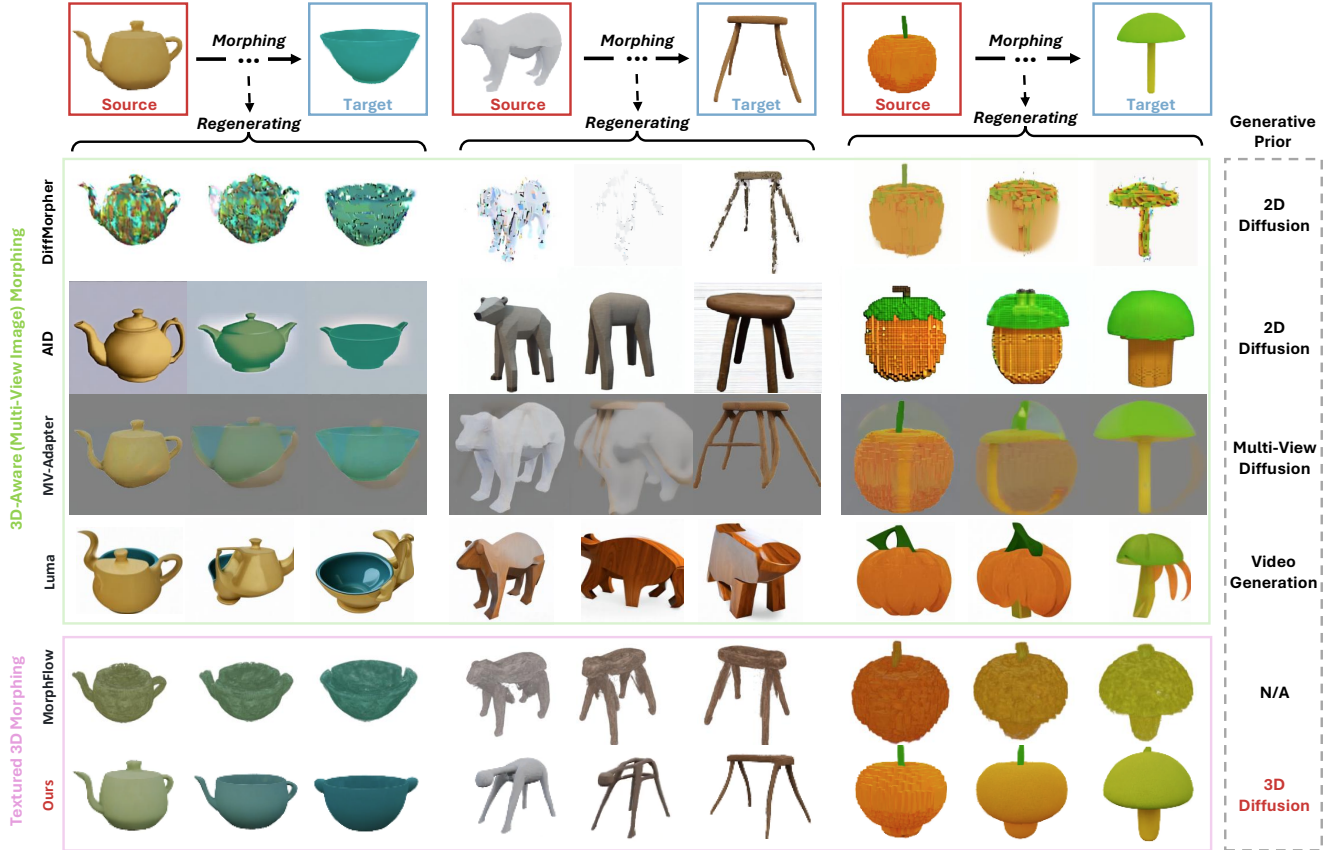


Fig. 6. Qualitative comparisons of different methods from tasks, morphing tricks, and generative priors. *More video results can be found here.*

z_G has a size of $M \times 3$ (with $M = 768$), and the corresponding feature z_T has dimensions $M \times 10$. All experiments use 250 denoising time steps. Fine-tuning is performed using LoRA models implemented with PEFT [Mangrulkar et al. 2022] using 500 training steps (rank=16, alpha=20, and list=['to_k', 'to_q', 'to_v', 'qkv']).

4.1.2 Morphing Configuration. In our experiments, the initial value of α is sampled from a Beta distribution over the $[0, 1]$ interval, with 10 points selected as interpolation weights. If multiple morphing is allowed, α can be concentrated in ranges with more variation by adjusting the Beta distribution or using the reschedule strategy from Diffmorpher. For Attention Fusion, we recommend starting from the first step, with geometry diffusion ending between steps 120 and 180, and texture diffusion finishing by step 5. For Token Reordering, it should begin at step 80 and end at step 200. For Low-Frequency Enhancement, the recommended time step range is from step 200 to step 230, while the $scale = 5$ and $\omega_0 = 0.1\pi$. *More details can be found in the **Supplementary Materials**.*

4.1.3 Baselines. (a) *Task (Textured 3D Morphing)*: Morphflow [Tsai et al. 2022] directly implements morphing on 3D volumetric representations; (b) *Morphing Tricks*: Diffmorpher [Zhang et al. 2024] and AID [He et al. 2024] propose fusion strategies for attention to enhance smoothness; (c) *Generative Priors*: We compare the performance of 2D diffusion (Diffmorpher, AID), multi-view diffusion

Table 1. Quantitative comparisons of different methods.

	Quantitative Metrics					User Study	
	FID↓	STP-GPT↑	SEP-GPT↑	PPL↓	PDV↓	STP-U↑	SEP-U↑
DiffMorpher	218.07	0.23	0.13	5.23	0.0535	0.435	0.300
AID	115.72	0.67	0.70	4.68	0.0118	0.380	0.505
MV-Adapter	120.93	0.63	0.57	7.29	0.0152	0.225	0.350
Luma	95.49	0.83	0.77	7.37	0.0007	0.415	0.330
MorphFlow	147.70	0.87	0.90	3.10	0.0001	0.555	0.505
Ours	6.36	1.00	1.00	3.02	0.0001	0.915	0.950

(MV-Adapter [Huang et al. 2024a]), video generation (Luma [AI 2025]), and 3D diffusion in the 3D morphing task.

4.1.4 Metrics. The performance of textured 3D morphing is evaluated using the following metrics: (a) *Fréchet Inception Distance (FID)* [Heusel et al. 2017]: Fidelity is measured by comparing 1,000 images rendered from original and interpolated 3D representations. (b) *Structural Plausibility-GPT (STP-GPT) and Semantic Plausibility-GPT (SEP-GPT)*: GPT-4o [OpenAI 2023] evaluates structural and semantic plausibility based on testing results, providing scores and explanations. (c) *Perceptual Path Length (PPL) and Perceptual Distance Variance (PDV)* [Zhang et al. 2024]: PPL sums perceptual losses over 20-frame sequences, reflecting smoothness and consistency, while PDV measures the variance, indicating transition homogeneity. (d) *Structural Plausibility-User (STP-U) and Semantic Plausibility-User*

(SEP-U): Volunteers score morphing results based on structural and semantic plausibility.

4.2 Evaluation

4.2.1 Textured 3D Morphing. Our method adopts a 3D generation prior for 3D morphing, offering two main benefits: direct morphing of textured 3D representations, and maintaining structural and semantic consistency in interpolated representations, as shown in Fig. 1 and Fig. 8. The closest baseline to our method is MorphFlow [Tsai et al. 2022], which morphs between two 3D volumetric representations using optimal transport optimization. However, as shown in Fig. 6 and Fig. 9, MorphFlow has two main drawbacks. First, the generated quality is low (See Tab.1); the advantage of volumetric representations for photorealism is diminished due to the dense interpolation process, which requires morphing even points with no color. Second, it lacks an effective generative prior to the intermediate process, limiting its ability to understand the semantic meaning of intermediate stages. As a result, it often introduces artifacts in morphing scenarios, such as generating six legs instead of four when morphing a bear’s and a table’s legs.

Our method not only significantly outperforms MorphFlow in quality but also demonstrates an impressive “understanding” when interpolating across diverse 3D object pairs from different categories. This understanding is evident in two key aspects: (a) the effective mapping of semantically similar parts, as shown when morphing a boot into a red teddy bear, where our model smoothly splits the boot into legs and transforms them into the bear’s facial features, and (b) minimal disconnected artifacts. The regenerative nature of our method ensures the fusion of source and target information while considering the distribution of the entire latent space, minimizing issues like 3D structure collapse or disconnected parts.

4.2.2 3D-Aware (Multi-View Image) Morphing. We evaluated alternatives to our method for textured 3D morphing from two perspectives. First, 3D morphing can be viewed as multi-view image morphing, where multi-view source and target images are fed into image morphing methods for pseudo-3D morphing. Second, many image and video generation models, beyond 3D priors, can perform interpolation tasks. Notably, 2D generation models [Huang et al. 2024a; Shi et al. 2023; Yang et al. 2024, 2023a,b], trained on larger datasets often produce 3D-consistent images with superior semantic, structural, and textural understanding compared to 3D models. Based on these insights, we explored three types of generative priors: 2D diffusion, multi-view diffusion, and video generation.

As shown in Fig. 6 and Tab. 1, compared to state-of-the-art 2D image morphing methods, such as DiffMorpher [Zhang et al. 2024] and AID [He et al. 2024], we found that 2D diffusion models often suffer from mode collapse when influenced by non-object image regions (e.g., DiffMorpher is sensitive to white backgrounds). Their lack of 3D consistency leads to inconsistent morphing results for the same α across different viewpoints. When comparing with multi-view diffusion models, we observed that their image-based multi-view generation is limited by pixel-aligned morphing. This limitation becomes apparent when matching pixels across large spatial distances—such as aligning a point on the lower edge of a pumpkin’s

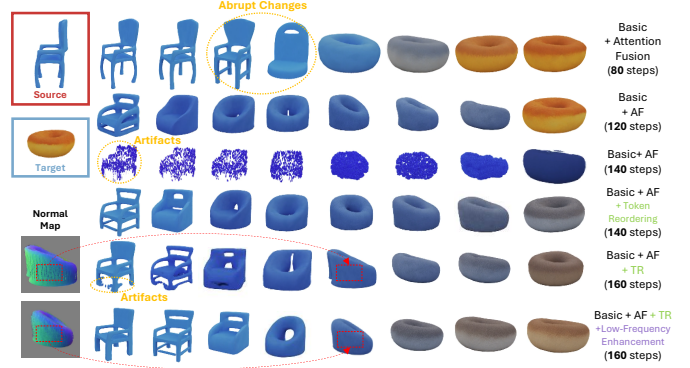


Fig. 7. Ablation experiments of our proposed strategies.

surface with a point on the stem of a mushroom in the image’s center, resulting in interpolation errors. Lastly, video generation models, while demonstrating strong spatial understanding and achieving morphing by specifying the source and target images as the first and last frames, suffer from limited controllability during generation, often producing incomplete or out-of-frame content. Additionally, the structural consistency of intermediate frames remains suboptimal.

4.3 Ablation Study

Balancing smooth transitions with structural plausibility (or overall generation quality) is challenging, especially in selecting the time step range for Attention Fusion. We empirically observe that texture diffusion allows for minimal attention fusion, while geometry diffusion offers a larger operational range, aligning well with the importance of shape understanding in 3D morphing. To address this, we incorporate Attention Fusion in texture diffusion from the first to the fifth time step, while progressively extending the final time step for geometry diffusion. Adding Attention Fusion on top of basic interpolation improves smoothness, but extending the final time step too far causes 3D structural collapse. Token Reordering helps mitigate this issue, though pushing the time step further reduces generative quality. Ultimately, by applying the Low-Frequency Enhancement strategy, we balance the smoothness and structural plausibility and ensure all frequencies are maintained effectively. More details can be found in Fig. 7 and **Supplementary Materials**.

5 Conclusions

We propose a method to achieve smooth and plausible morphing sequences across diverse cross-category 3D object pairs, incorporating Attention Fusion, Token Reordering, and Low-Frequency Enhancement. This introduces a new paradigm for textured 3D morphing, extending beyond the limitations of previous research confined to shape-only morphing on topologically aligned datasets.

Discussions. Our future work will focus on morphing more complex textured 3D objects, exploring two main directions: (a) Enhancing fidelity and diversity using advanced 3D generation models like Trellis [Xiang et al. 2024], and (b) Expanding morphing to generate complex sequences, such as few-shot motion interpolation [Shen et al. 2024], while maintaining temporal consistency. Additionally, we aim to explore the transitions for 4D content like the “Birth and Death of a Rose” [Geng et al. 2024].

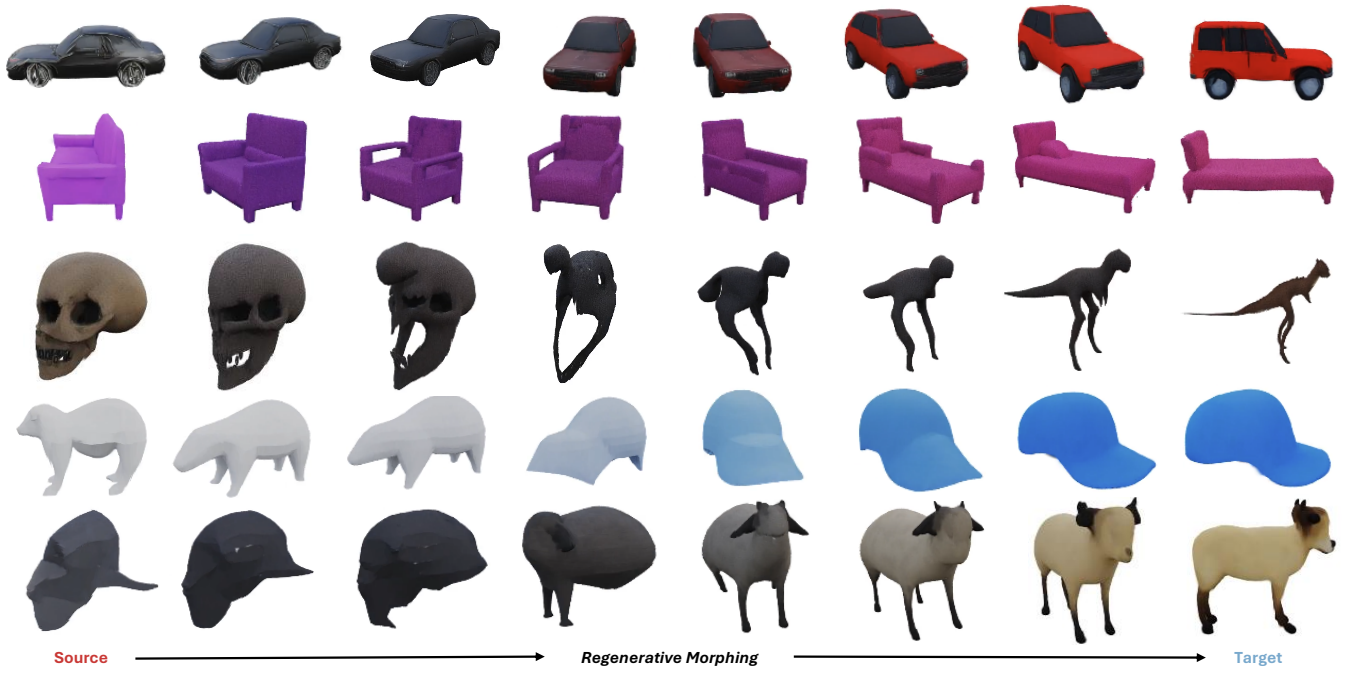


Fig. 8. More 3D morphing sequences generated by our method.

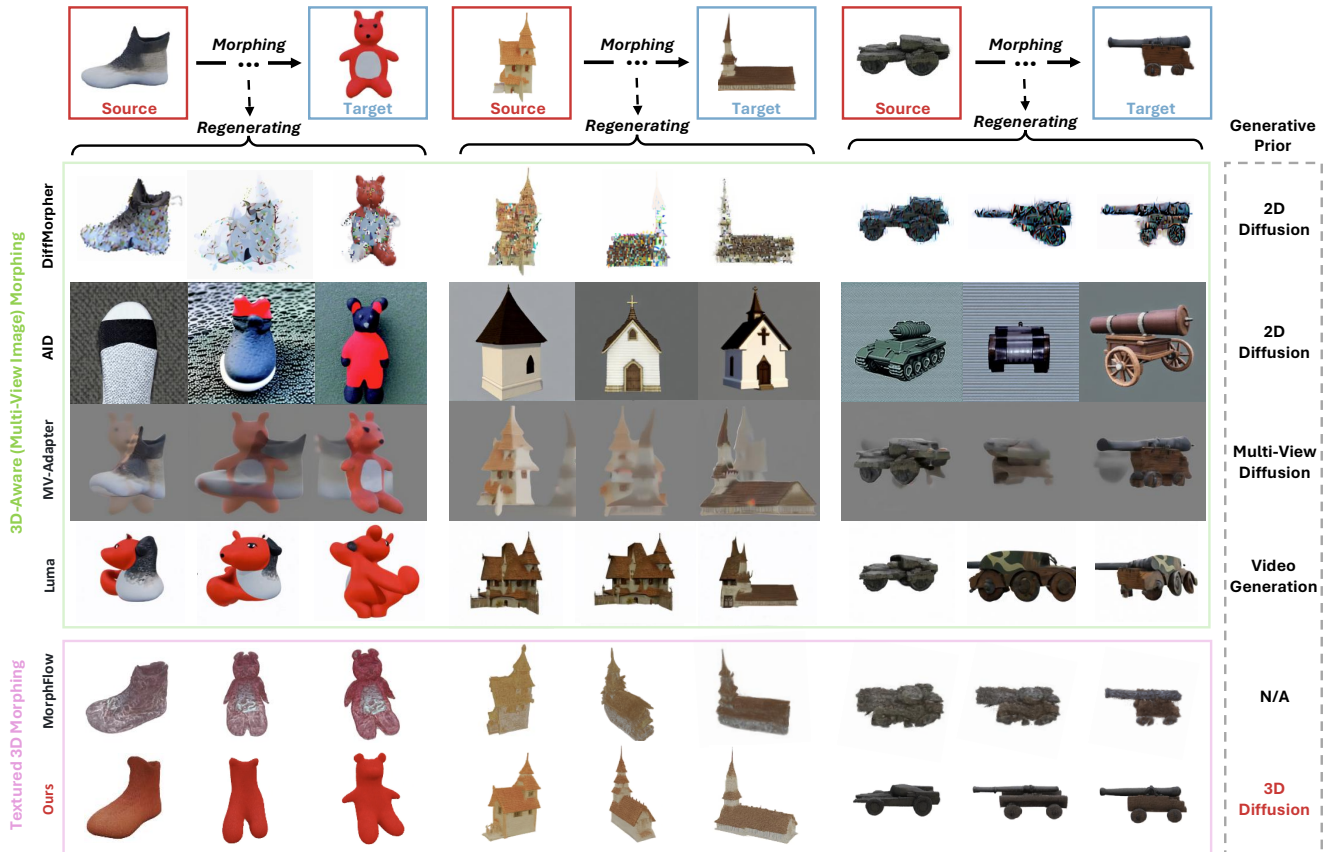


Fig. 9. More qualitative comparisons of different methods from tasks, morphing tricks, and generative priors. *More video results can be found [here](#).*

References

- Ahmed Abdelreheem, Ivan Skorokhodov, Maks Ovsjanikov, and Peter Wonka. 2023. Satr: Zero-shot semantic segmentation of 3d shapes. In *Proceedings of the IEEE/CVF International Conference on Computer Vision*. 15166–15179.
- Luma Labs AI. 2025. Luma Dream Machine: AI-Powered Video Content Creation. <https://dream-machine.lumalabs.ai/>. Accessed: 2025-01-15.
- Michael S Albergo, Nicholas M Boffi, and Eric Vanden-Eijnden. 2023. Stochastic interpolants: A unifying framework for flows and diffusions. *arXiv preprint arXiv:2303.08797* (2023).
- Alyaa Qusay Aloraibi. 2023. Image morphing techniques: A review. (2023).
- Hadar Averbuch-Elor, Daniel Cohen-Or, and Johannes Kopf. 2016. Smooth image sequences for data-driven morphing. In *computer graphics forum*, Vol. 35. Wiley Online Library, 203–213.
- Melike Aydinlar and Yusuf Sahillioglu. 2021. Part-based data-driven 3D shape interpolation. *Computer-Aided Design* 136 (2021), 103027.
- Thaddeus Beier and Shawn Neely. 2023. Feature-based image metamorphosis. In *Seminal Graphics Papers: Pushing the Boundaries, Volume 2*. 529–536.
- Bhumika G Bhatt. 2011. Comparative study of triangulation based and feature based image morphing. *Signal & Image Processing* 2, 4 (2011), 235.
- Federica Bogo, Javier Romero, Matthew Loper, and Michael J Black. 2014. FAUST: Dataset and evaluation for 3D mesh registration. In *Proceedings of the IEEE conference on computer vision and pattern recognition*. 3794–3801.
- Junsong Chen, Jincheng Yu, Chongjian Ge, Lewei Yao, Enze Xie, Yue Wu, Zhongdao Wang, James Kwok, Ping Luo, Huchuan Lu, et al. 2024b. Pixart- α : Fast training of diffusion transformer for photorealistic text-to-image synthesis. *ICLR* (2024).
- Zhaoxi Chen, Jiayang Tang, Yuhao Dong, Ziang Cao, Fangzhou Hong, Yushi Lan, Tengfei Wang, Haozhe Xie, Tong Wu, Shunsuke Saito, et al. 2024a. 3dtopia-xl: Scaling high-quality 3d asset generation via primitive diffusion. *arXiv preprint arXiv:2409.12957* (2024).
- Soheil Darabi, Eli Shechtman, Connelly Barnes, Dan B Goldman, and Pradeep Sen. 2012. Image melding: Combining inconsistent images using patch-based synthesis. *ACM Transactions on graphics (TOG)* 31, 4 (2012), 1–10.
- Matt Deitke, Dustin Schwenk, Ping Luo, Huchuan Lu, Luca Weihs, Oscar Michel, Eli VanderBilt, Ludwig Schmidt, Kiana Ehsani, Aniruddha Kembhavi, and Ali Farhadi. 2023. Objaverse: A universe of annotated 3d objects. In *Proceedings of the IEEE/CVF Conference on Computer Vision and Pattern Recognition*. 13142–13153.
- Jiacheng Deng, Chuxin Wang, Jiahao Lu, Jianfeng He, Tianzhu Zhang, Jiyang Yu, and Zhe Zhang. 2023. Se-ornet: Self-ensembling orientation-aware network for unsupervised point cloud shape correspondence. In *Proceedings of the IEEE/CVF Conference on Computer Vision and Pattern Recognition*. 5364–5373.
- Roberto M Dyke, Yu-Kun Lai, Paul L Rosin, Stefano Zappalà, Seana Dykes, Daoliang Guo, Kun Li, Riccardo Marin, Simone Melzi, and Jingyu Yang. 2020. SHREC'20: Shape correspondence with non-isometric deformations. *Computers & Graphics* 92 (2020), 28–43.
- Michal Edelman, Danielle Ezuz, and Mirela Ben-Chen. 2019. Enigma: Evolutionary non-isometric geometry matching. *arXiv preprint arXiv:1905.10763* (2019).
- Marvin Eisenberger, Zorah Lahner, and Daniel Cremers. 2020. Smooth shells: Multi-scale shape registration with functional maps. In *Proceedings of the IEEE/CVF Conference on Computer Vision and Pattern Recognition*. 12265–12274.
- Marvin Eisenberger, David Novotny, Gael Kerchenbaum, Patrick Labatut, Natalia Neverova, Daniel Cremers, and Andrea Vedaldi. 2021. Neuromorph: Unsupervised shape interpolation and correspondence in one go. In *Proceedings of the IEEE/CVF Conference on Computer Vision and Pattern Recognition*. 7473–7483.
- Noa Fish, Richard Zhang, Lilach Perry, Daniel Cohen-Or, Eli Shechtman, and Connelly Barnes. 2020. Image morphing with perceptual constraints and stn alignment. In *Computer Graphics Forum*, Vol. 39. Wiley Online Library, 303–313.
- Lawson Fulton, Vismay Modi, David Duvenaud, David IW Levin, and Alec Jacobson. 2019. Latent-space dynamics for reduced deformable simulation. In *Computer graphics forum*, Vol. 38. Wiley Online Library, 379–391.
- William Gao, Noam Aigerman, Thibault Groueix, Vova Kim, and Rana Hanocka. 2023. Textdeformer: Geometry manipulation using text guidance. In *ACM SIGGRAPH 2023 Conference Proceedings*. 1–11.
- Chen Geng, Yunzhi Zhang, Shanzhe Wu, and Jiajun Wu. 2024. Birth and Death of a Rose. [arXiv:2412.05278 \[cs.CV\]](https://arxiv.org/abs/2412.05278) <https://arxiv.org/abs/2412.05278>
- Ayaan Haque, Matthew Tancik, Alexei A Efros, Aleksander Holynski, and Angjoo Kanazawa. 2023. Instruct-nerf2nerf: Editing 3d scenes with instructions. In *Proceedings of the IEEE/CVF International Conference on Computer Vision*. 19740–19750.
- Qiyuan He, Jinghao Wang, Ziwei Liu, and Angela Yao. 2024. AID: Attention Interpolation of Text-to-Image Diffusion. *NeurIPS* (2024).
- Eric Hedlin, Gopal Sharma, Shweta Mahajan, Hossam Isack, Abhishek Kar, Andrea Tagliasacchi, and Kwang Moo Yi. 2024. Unsupervised semantic correspondence using stable diffusion. *Advances in Neural Information Processing Systems* 36 (2024).
- Martin Heusel, Hubert Ramsauer, Thomas Unterthiner, Bernhard Nessler, and Sepp Hochreiter. 2017. Gans trained by a two time-scale update rule converge to a local nash equilibrium. *Advances in neural information processing systems* 30 (2017).
- Edward J Hu, Yelong Shen, Phillip Wallis, Zeyuan Allen-Zhu, Yuanzhi Li, Shean Wang, Lu Wang, and Weizhu Chen. 2021. Lora: Low-rank adaptation of large language models. *arXiv preprint arXiv:2106.09685* (2021).
- Binbin Huang, Zehao Yu, Anpei Chen, Andreas Geiger, and Shenghua Gao. 2024c. 2d gaussian splatting for geometrically accurate radiance fields. In *ACM SIGGRAPH 2024 conference papers*. 1–11.
- Zehuan Huang, Yuanchen Guo, Haoran Wang, Ran Yi, Lizhuang Ma, Yan-Pei Cao, and Lu Sheng. 2024a. MV-Adapter: Multi-view Consistent Image Generation Made Easy. *arXiv preprint arXiv:2412.03632* (2024).
- Zixuan Huang, Justin Johnson, Shoubhik Debnath, James M Rehg, and Chao-Yuan Wu. 2024b. PointInfinity: Resolution-Invariant Point Diffusion Models. In *Proceedings of the IEEE/CVF Conference on Computer Vision and Pattern Recognition*. 10050–10060.
- Alec Jacobson, Zhigang Deng, Ladislav Kavan, and John P Lewis. 2014. Skinning: Real-time shape deformation (full text not available). In *ACM SIGGRAPH 2014 Courses*. 1–1.
- Hyunwoo Kim, Itai Lang, Noam Aigerman, Thibault Groueix, Vladimir G Kim, and Rana Hanocka. 2024. MeshUp: Multi-Target Mesh Deformation via Blended Score Distillation. *arXiv preprint arXiv:2408.14899* (2024).
- Vladimir G Kim, Yaron Lipman, and Thomas Funkhouser. 2011. Blended intrinsic maps. *ACM transactions on graphics (TOG)* 30, 4 (2011), 1–12.
- Yushi Lan, Fangzhou Hong, Shuai Yang, Shangchen Zhou, Xuyi Meng, Bo Dai, Xingang Pan, and Chen Change Loy. 2025a. Ln3diff: Scalable latent neural fields diffusion for speedy 3d generation. In *European Conference on Computer Vision*. Springer, 112–130.
- Yushi Lan, Chen Change Loy, and Bo Dai. 2022. DDF: Correspondence Distillation from NeRF-based GAN. *IJCV* (2022).
- Yushi Lan, Shangchen Zhou, Zhaoyang Lyu, Fangzhou Hong, Shuai Yang, Bo Dai, Xingang Pan, and Chen Change Loy. 2025b. GaussianAnything: Interactive Point Cloud Latent Diffusion for 3D Generation. In *ICLR*.
- Jing Liao, Rodolfo S Lima, Diego Nehab, Hugues Hoppe, Pedro V Sander, and Jinhui Yu. 2014. Automating image morphing using structural similarity on a halfway domain. *ACM Transactions on Graphics (TOG)* 33, 5 (2014), 1–12.
- Jianchu Lin, Yinxi Gu, Guangxiao Du, Guoqiang Qu, Xiaobing Chen, Yudong Zhang, Shangbing Gao, Zhen Liu, and Nallappan Gunasekaran. 2024. 2D/3D Image morphing technology from traditional to modern: A survey. *Information Fusion* (2024), 102913.
- Yaron Lipman, Ricky TQ Chen, Heli Ben-Hamu, Maximilian Nickel, and Matt Le. 2022. Flow matching for generative modeling. *arXiv preprint arXiv:2210.02747* (2022).
- Sourab Mangrulkar, Sylvain Gugger, Lysandre Debut, Younes Belkada, Sayak Paul, and Benjamin Bossan. 2022. PEFT: State-of-the-art Parameter-Efficient Fine-Tuning methods. <https://github.com/huggingface/peft>.
- Oscar Michel, Roi Bar-On, Richard Liu, Sagie Benaim, and Rana Hanocka. 2022. Text2mesh: Text-driven neural stylization for meshes. In *Proceedings of the IEEE/CVF Conference on Computer Vision and Pattern Recognition*. 13492–13502.
- Nasir Mohammad Khalid, Tianhao Xie, Eugene Belilovsky, and Tiberiu Popa. 2022. Clip-mesh: Generating textured meshes from text using pretrained image-text models. In *SIGGRAPH Asia 2022 conference papers*. 1–8.
- Luca Morreale, Noam Aigerman, Vladimir G Kim, and Niloy J Mitra. 2024. Neural semantic surface maps. In *Computer Graphics Forum*, Vol. 43. Wiley Online Library, e15005.
- OpenAI. 2023. GPT-4: OpenAI’s Fourth-Generation Language Model. <https://openai.com/research/gpt-4>
- Maxime Oquab, Timothée Darcet, Théo Moutakanni, Huy Vo, Marc Szafraniec, Vasil Khalidov, Pierre Fernandez, Daniel Haziza, Francisco Massa, Alaaeldin El-Nouby, et al. 2023. Dinov2: Learning robust visual features without supervision. *arXiv preprint arXiv:2304.07193* (2023).
- Maks Ovsjanikov, Mirela Ben-Chen, Justin Solomon, Adrian Butscher, and Leonidas Guibas. 2012. Functional maps: a flexible representation of maps between shapes. *ACM Transactions on Graphics (ToG)* 31, 4 (2012), 1–11.
- William Peebles and Saining Xie. 2023. Scalable diffusion models with transformers. In *Proceedings of the IEEE/CVF International Conference on Computer Vision*. 4195–4205.
- Ben Poole, Ajay Jain, Jonathan T Barron, and Ben Mildenhall. 2022. Dreamfusion: Text-to-3d using 2d diffusion. *arXiv preprint arXiv:2209.14988* (2022).
- Alec Radford, Jong Wook Kim, Chris Hallacy, Aditya Ramesh, Gabriel Goh, Sandhini Agarwal, Girish Sastry, Amanda Askell, Pamela Mishkin, Jack Clark, et al. 2021. Learning transferable visual models from natural language supervision. In *International conference on machine learning*. PMLR, 8748–8763.
- Jing Ren, Simone Melzi, Maks Ovsjanikov, and Peter Wonka. 2020. Maptree: Recovering multiple solutions in the space of maps. *ACM Transactions on Graphics* 39, 6 (2020), 1–17.
- Robin Rombach, Andreas Blattmann, Dominik Lorenz, Patrick Esser, and Björn Ommer. 2022. High-resolution image synthesis with latent diffusion models. In *Proceedings of the IEEE/CVF conference on computer vision and pattern recognition*. 10684–10695.
- Chitwan Saharia, William Chan, Saurabh Saxena, Lala Li, Jay Whang, Emily L Denton, Kamyar Ghasemipour, Raphael Gontijo Lopes, Burcu Karagol Ayan, Tim Salimans,

- et al. 2022. Photorealistic text-to-image diffusion models with deep language understanding. *Advances in neural information processing systems* 35 (2022), 36479–36494.
- Mehdi SM Sajjadi, Henning Meyer, Etienne Pot, Urs Bergmann, Klaus Greff, Noha Radwan, Suhani Vora, Mario Lukić, Daniel Duckworth, Alexey Dosovitskiy, et al. 2022. Scene representation transformer: Geometry-free novel view synthesis through set-latent scene representations. In *Proceedings of the IEEE/CVF Conference on Computer Vision and Pattern Recognition*. 6229–6238.
- Dvir Samuel, Rami Ben-Ari, Nir Darshan, Haggai Maron, and Gal Chechik. 2024. Norm-guided latent space exploration for text-to-image generation. *Advances in Neural Information Processing Systems* 36 (2024).
- Eli Shechtman, Alex Rav-Acha, Michal Irani, and Steve Seitz. 2010. Regenerative morphing. In *2010 IEEE Computer Society Conference on Computer Vision and Pattern Recognition*. IEEE, 615–622.
- Liao Shen, Tianqi Liu, Huiqiang Sun, Xinyi Ye, Baopu Li, Jianming Zhang, and Zhiguo Cao. 2024. Dreammover: Leveraging the prior of diffusion models for image interpolation with large motion. *arXiv preprint arXiv:2409.09605* 2 (2024).
- Yichun Shi, Peng Wang, Jianglong Ye, Mai Long, Kejie Li, and Xiao Yang. 2023. Mvdream: Multi-view diffusion for 3d generation. *arXiv preprint arXiv:2308.16512* (2023).
- Chenyang Si, Ziqi Huang, Yuming Jiang, and Ziwei Liu. 2024. Freeu: Free lunch in diffusion u-net. In *Proceedings of the IEEE/CVF Conference on Computer Vision and Pattern Recognition*. 4733–4743.
- Justin Solomon, Fernando De Goes, Gabriel Peyré, Marco Cuturi, Adrian Butscher, Andy Nguyen, Tao Du, and Leonidas Guibas. 2015. Convolutional wasserstein distances: Efficient optimal transportation on geometric domains. *ACM Transactions on Graphics (ToG)* 34, 4 (2015), 1–11.
- Jiaming Song, Chenlin Meng, and Stefano Ermon. 2020. Denoising diffusion implicit models. *arXiv preprint arXiv:2010.02502* (2020).
- Olga Sorkine and Marc Alexa. 2007. As-rigid-as-possible surface modeling. In *Symposium on Geometry processing*, Vol. 4. Citeseer, 109–116.
- Olga Sorkine, Daniel Cohen-Or, Yaron Lipman, Marc Alexa, Christian Rössl, and H-P Seidel. 2004. Laplacian surface editing. In *Proceedings of the 2004 Eurographics/ACM SIGGRAPH symposium on Geometry processing*. 175–184.
- Mingze Sun, Chen Guo, Puhua Jiang, Shiwei Mao, Yurun Chen, and Ruqi Huang. 2024. SRIF: Semantic Shape Registration Empowered by Diffusion-based Image Morphing and Flow Estimation. In *SIGGRAPH Asia 2024 Conference Papers*. 1–11.
- Gary KL Tam, Zhi-Quan Cheng, Yu-Kun Lai, Frank C Langbein, Yonghuai Liu, David Marshall, Ralph R Martin, Xian-Fang Sun, and Paul L Rosin. 2012. Registration of 3D point clouds and meshes: A survey from rigid to nonrigid. *IEEE transactions on visualization and computer graphics* 19, 7 (2012), 1199–1217.
- Luming Tang, Menglin Jia, Qianqian Wang, Cheng Perng Phoo, and Bharath Hariharan. 2023. Emergent correspondence from image diffusion. *Advances in Neural Information Processing Systems* 36 (2023), 1363–1389.
- Chih-Jung Tsai, Cheng Sun, and Hwann-Tzong Chen. 2022. Multiview Regenerative Morphing with Dual Flows. In *European Conference on Computer Vision*. Springer, 492–509.
- Arash Vahdat, Francis Williams, Zan Gojic, Or Litany, Sanja Fidler, Karsten Kreis, et al. 2022. Lion: Latent point diffusion models for 3d shape generation. *Advances in Neural Information Processing Systems* 35 (2022), 10021–10039.
- A Vaswani. 2017. Attention is all you need. *Advances in Neural Information Processing Systems* (2017).
- Shantanu Vyas, Ting-Ju Chen, Ronak R Mohanty, Peng Jiang, and Vinayak R Krishnamurthy. 2021. Latent embedded graphs for image and shape interpolation. *Computer-Aided Design* 140 (2021), 103091.
- George Wolberg. 1998. Image morphing: a survey. *The visual computer* 14, 8-9 (1998), 360–372.
- Tianxing Wu, Chenyang Si, Yuming Jiang, Ziqi Huang, and Ziwei Liu. 2025. Freeinit: Bridging initialization gap in video diffusion models. In *European Conference on Computer Vision*. Springer, 378–394.
- Jianfeng Xiang, Zelong Lv, Sicheng Xu, Yu Deng, Ruicheng Wang, Bowen Zhang, Dong Chen, Xin Tong, and Jialong Yang. 2024. Structured 3D Latents for Scalable and Versatile 3D Generation. *arXiv preprint arXiv:2412.01506* (2024).
- Jiale Xu, Weihao Cheng, Yiming Gao, Xintao Wang, Shenghua Gao, and Ying Shan. 2024. Instantmesh: Efficient 3d mesh generation from a single image with sparse-view large reconstruction models. *arXiv preprint arXiv:2404.07191* (2024).
- Songlin Yang, Wei Wang, Yushi Lan, Xiangyu Fan, Bo Peng, Lei Yang, and Jing Dong. 2024. Learning dense correspondence for nerf-based face reenactment. In *Proceedings of the AAAI Conference on Artificial Intelligence*, Vol. 38. 6522–6530.
- Songlin Yang, Wei Wang, Jun Ling, Bo Peng, Xu Tan, and Jing Dong. 2023a. Context-aware talking-head video editing. In *Proceedings of the 31st ACM International Conference on Multimedia*. 7718–7727.
- Songlin Yang, Wei Wang, Bo Peng, and Jing Dong. 2023b. Designing a 3D-aware StyleNeRF encoder for face editing. In *ICASSP 2023-2023 IEEE International Conference on Acoustics, Speech and Signal Processing (ICASSP)*. IEEE, 1–5.
- Sihyun Yu, Sangkyung Kwak, Huiwon Jang, Jongheon Jeong, Jonathan Huang, Jinwoo Shin, and Saining Xie. 2024. Representation alignment for generation: Training diffusion transformers is easier than you think. *arXiv preprint arXiv:2410.06940* (2024).
- Mehmet Ersin Yumer, Siddhartha Chaudhuri, Jessica K Hodgins, and Levent Burak Kara. 2015. Semantic shape editing using deformation handles. *ACM Transactions on Graphics (TOG)* 34, 4 (2015), 1–12.
- Xiao Zhan, Rao Fu, and Daniel Ritchie. 2024. CharacterMixer: Rig-Aware Interpolation of 3D Characters. In *Computer Graphics Forum*. Wiley Online Library, e15047.
- Biao Zhang, Jiapeng Tang, Matthias Niessner, and Peter Wonka. 2023. 3dshape2vecset: A 3d shape representation for neural fields and generative diffusion models. *ACM Transactions on Graphics (TOG)* 42, 4 (2023), 1–16.
- Kaiwen Zhang, Yifan Zhou, Xudong Xu, Bo Dai, and Xingang Pan. 2024. DiffMorpher: Unleashing the Capability of Diffusion Models for Image Morphing. In *Proceedings of the IEEE/CVF Conference on Computer Vision and Pattern Recognition*. 7912–7921.
- Zhengbo Zhang, Li Xu, Duo Peng, Hossein Rahmani, and Jun Liu. 2025. Diff-tracker: text-to-image diffusion models are unsupervised trackers. In *European Conference on Computer Vision*. Springer, 319–337.
- Junzhe Zhu, Yuanchen Ju, Junyi Zhang, Muhan Wang, Zhecheng Yuan, Kaizhe Hu, and Huazhe Xu. 2024. DenseMatcher: Learning 3D Semantic Correspondence for Category-Level Manipulation from a Single Demo. *arXiv preprint arXiv:2412.05268* (2024).
- Bhushan Zope and Soniya B Zope. 2017. A Survey of Morphing Techniques. *International Journal of Advanced Engineering, Management and Science* 3, 2 (2017), 239773.

A Supplementary Materials

A.1 Outline

To experimentally validate the rationale behind the motivations discussed in our manuscript and to provide additional details that could not be elaborated on due to manuscript space limitations, we have carefully prepared comprehensive supplementary materials for reference (*Click on the index to directly access the corresponding content*).

- A.2 3D Generation Model: Gaussian Anything
- A.3 How to Align/Prepare the Input 3D and Images with Gaussian Anything?
- A.4 How to Choose Appropriate 3D Diffusion Models for 3D Morphing?
- A.5 Effects of Scale in the Low-Frequency Enhancement
- A.6 Baseline Methods and Implementation Details
- A.7 Comparisons with Shape Morphing Methods
- A.8 Exploratory Experiments with Explicit Correspondence
- A.9 Testing Protocol and Cases
- A.10 Raw Statistics of User Study

A.2 3D Generation Model: Gaussian Anything

Gaussian Anything [Lan et al. 2025b] introduces a 3D generation framework built on a point cloud-based 3D latent space. The 3D Variational Autoencoder (VAE) (See A.2.1) efficiently encodes 3D data into a dynamic latent space, which is subsequently decoded into detailed Surfel Gaussians. Diffusion models (See A.2.2) trained on this compacted latent space achieve remarkable results in 3D generation and editing conditioned on text, as well as in generating high-quality 3D content from images on diverse real-world datasets. For more implementation details, please see their [project page](#).

A.2.1 Point-Cloud Structured 3D VAE. A 3D VAE is introduced that takes multi-view posed RGB-D (Depth)-Normal renderings as input. These renderings are easy to generate and provide a rich set of 3D attributes corresponding to the input object. Each view’s information is concatenated along the channel dimension and efficiently encoded using a scene representation transformer [Sajjadi et al. 2022], producing a compact latent representation of the 3D input. Rather than directly applying this latent representation to diffusion learning, the model’s innovative method transforms unordered tokens into a shape that mirrors the 3D input. This transformation is achieved by cross-attending [Huang et al. 2024b] the latent set with a sparse point cloud sampled from the 3D shape. This point-cloud structured latent space significantly aids in disentangling shape and texture, as well as enabling 3D editing. Subsequently, a DiT-based 3D decoder [Peebles and Xie 2023] progressively decodes and upscales the latent point cloud into a dense set of Surfel Gaussians [Huang et al. 2024c], which are rasterized into high-resolution renderings to guide the 3D VAE training.

A.2.2 Cascaded 3D Generation with Flow Matching. After the 3D VAE is trained, they conduct cascaded latent diffusion modeling on the latent space through flow matching [Albergo et al. 2023] using the DiT [Peebles and Xie 2023] framework. To encourage better shape-texture disentanglement, a point cloud diffusion model is first trained to carve the overall layout of the input shape. Then,

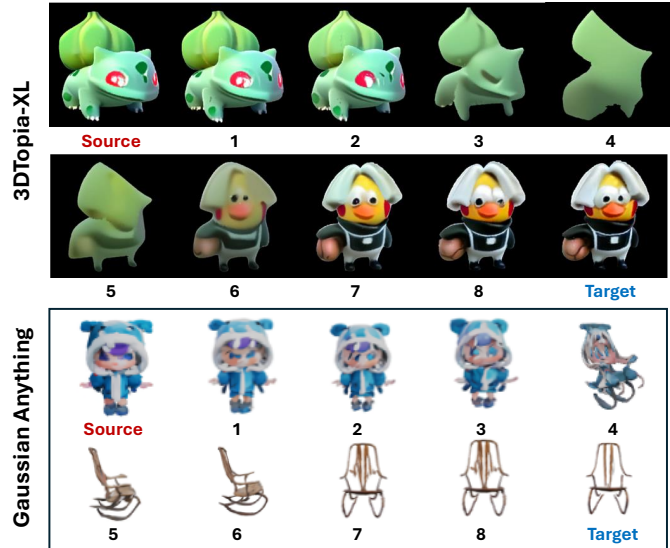


Fig. 10. Evaluation of 3D generation model capabilities. Based on accessibility, we tested the interpolation performance of projects with available training code and model details, namely 3DTopia-XL [Chen et al. 2024a] and Gaussian Anything [Lan et al. 2025b] in the image-to-3D setting. We found that while 3DTopia-XL generates high-quality 3D assets, its latent space lacks reasonable generative capabilities, as evidenced by the interpolation results between the 3rd and 6th samples.

a point cloud feature diffusion model is cascaded to output the corresponding feature conditioned on the generated point cloud. The generated featured point cloud is then decoded into Surfel Gaussians [Huang et al. 2024c] via pre-trained VAE for downstream applications.

A.3 How to Align/Prepare the Input 3D and Images with Gaussian Anything?

For textured 3D representations, multi-view RGB, depth, and normal images can be directly rendered, and then the corresponding latent can be obtained using the 3D VAE of Gaussian Anything. For a single image, two methods are possible: (a) The 2D image can be lifted to multi-view using a multi-view generation model [Shi et al. 2023], and then a renderable textured 3D model can be trained from these multi-view images, or (b) A direct image-to-3D method [Huang et al. 2024a] can be used to obtain the textured 3D model.

A.4 How to Choose Appropriate 3D Diffusion Models for 3D Morphing?

Selecting an appropriate 3D generative model is foundational for textured 3D regenerative morphing, as it determines (a) the range of 3D object categories that can be handled and (b) the ability to integrate diverse information for generating smooth interpolation sequences. We followed four criteria when selecting a 3D generative model for our research:

(a) **Accessibility:** Training 3D generative models is highly resource-intensive, and high-quality models capable of generating diverse



Fig. 11. The effects of *scale* in the Low-Frequency Enhancement.

outputs are often proprietary assets, accessible only through APIs. This limits our ability to probe the internal characteristics and potential issues of such models. Therefore, an ideal 3D generative model should be open-sourced, including all testing and training files, datasets, and model checkpoints. Based on this criterion, we selected Gaussian Anything [Lan et al. 2025b] and 3DTopia-XL [Chen et al. 2024a] as our potential target models.

(b) Fairness: For data-driven studies, fairness is reflected in the use of publicly available datasets for training, ensuring future researchers can build on our work with a well-established baseline or benchmark. The Objaverse [Deitke et al. 2023] dataset, currently one of the most widely adopted 3D datasets, is particularly suitable for academic research. Thus, we prefer Gaussian Anything [Lan et al. 2025b], which is trained on Objaverse.

(c) Generation Quality: 3D generative modeling has become one of the most competitive and rapidly evolving research areas in recent years, with many papers showcasing impressive results. However, unlike 2D images or videos, 3D training data is harder to collect at scale, and no existing model can perfectly generate a full range of 3D objects. Therefore, we prioritized models capable of generating a wide variety of objects, ideally including categories such as animals, buildings, furniture, food, transportation, and plants. After evaluating the performance of several state-of-the-art 3D generative models on image-to-3D and text-to-3D tasks, we selected Gaussian Anything [Lan et al. 2025b] as our research model.

(d) Preliminary Interpolation Feasibility: For models with strong generative capabilities, the quickest way to determine their suitability for 3D morphing research is to conduct basic interpolation tests. Not all generative models can effectively fuse different information for interpolation. Among the tested models (as shown in Fig. 10), Gaussian Anything [Lan et al. 2025b] demonstrated the best interpolation performance, making it the most suitable choice for our study.

A.5 Effects of Scale in the Low-Frequency Enhancement

As shown in Fig. 11, increasing the scale continuously enhances the surface generation capability. However, through empirical observation, we found that beyond a certain value, the surface does not increase further with larger scale values. Therefore, setting the scale to 5 is optimal.

A.6 Baseline Methods and Implementation Details

A.6.1 DiffMorpher. Given two images, DiffMorpher [Zhang et al. 2024] uses two LoRAs [Hu et al. 2021] to fit the two images respectively. Then the latent noises for the two images are obtained via

DDIM inversion [Song et al. 2020]. The mean and standard deviation of the interpolated noises are adjusted through AdaIN. To generate an intermediate image, they interpolate between both the LoRA parameters and the latent noises via the interpolation ratio α . In addition, the text embedding and the K and V in self-attention modules are also replaced with the interpolation between the corresponding components. Using a sequence of α and a new sampling schedule, their method will produce a series of high-fidelity images depicting a smooth transition between the two given images. We followed the script and default parameter settings given by DiffMorpher and used their [open-source code](#) to produce the results.

A.6.2 AID. Similar to the DiffMorpher [Zhang et al. 2024] framework, AID [He et al. 2024] removes the LoRA fitting and introduces the following additional modifications: (a) Replacing both cross-attention and self-attention mechanisms during interpolated image generation with fused interpolated attention; (b) Selecting interpolation coefficients using a Beta prior; (c) Injecting prompt guidance into the fused interpolated cross-attention. We implemented the generation of relevant results based on the code of Stable Diffusion 1.5 [Rombach et al. 2022], and all settings follow the default settings of AID. More details can be found on their [project page](#).

A.6.3 MV-Adapter. MV-Adapter [Huang et al. 2024a] is a versatile plug-and-play and state-of-the-art adapter that turns existing pre-trained text-to-image (T2I) diffusion models to multi-view image generators. We generated image morphing results based on their Image-to-Multiview [code](#) and Stable Diffusion 2.1. The only change is that we linearly interpolated the condition features of the source image and target image extracted by their image encoder according to different morphing weights.

A.6.4 Luma. The [Dream Machine](#) of Luma AI is based on the DiT [Peebles and Xie 2023] video generation architecture, capable of generating high-quality videos with 120 frames in just 120 seconds, enabling rapid creative iteration. It understands physical interactions, ensuring that the generated video characters and scenes maintain consistency and physical accuracy. We accessed their API and utilized the video generation function to generate intermediate video frames by providing the source image as the first frame and the target image as the last frame. For instance, for the "polar bear" to "wooden stool" morphing video generation, the guiding prompt we used is: "*Morph a polar bear into a wooden stool, smoothly interpolating both geometry and texture, with the object always remaining at the center of the frame.*"

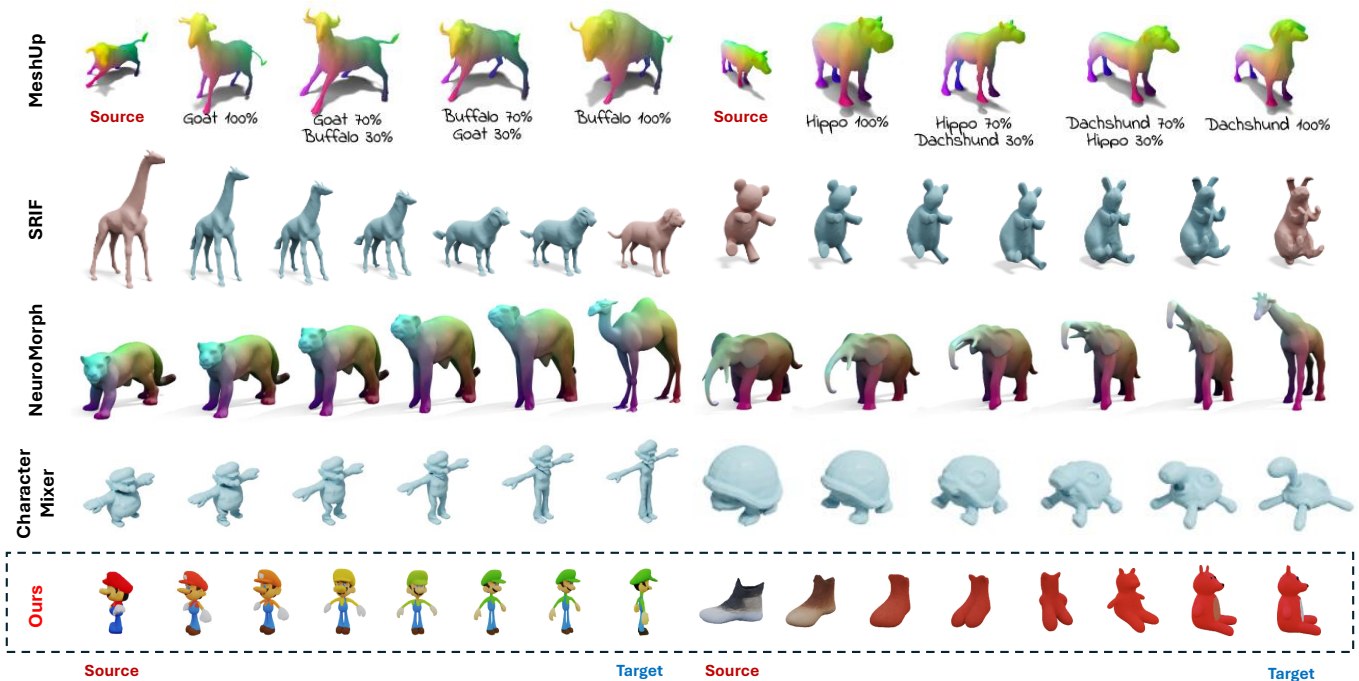


Fig. 12. Comparison of related methods. Our method focuses on textured 3D morphing, whereas MeshUp [Kim et al. 2024], SRIF [Sun et al. 2024], NeuroMorph [Eisenberger et al. 2021], and CharacterMixer [Zhan et al. 2024] are limited to shape-only 3D morphing. Note that all results outside the dashed boxes are sourced from their respective manuscripts.

Table 2. Task setting comparison.

	Shape	Texture	Aligned Dataset	Out-of-Domain Morphing
MeshUp	✓	×	No Need	✓
SRIF	✓	×	No Need	✓
NeuroMorph	✓	×	Need	×
CharacterMixer	✓	×	Need	×
MorphFlow	✓	✓	No Need	✓
Ours	✓	✓	No Need	✓

A.6.5 MorphFlow. MorphFlow [Tsai et al. 2022] introduces an optimization-based method for multi-view regenerative morphing. The method does not assume prior knowledge of the categories or affinities between the source and target images, nor does it rely on predefined correspondences. By utilizing optimal transport, the method interpolates a volume for rendering smooth multi-view transitions. Additionally, a rigid transformation is incorporated to preserve structure during the morphing process. The method is highly efficient, learning and rendering a morphing renderer from scratch in just 30 minutes, with the ability to generate a novel-view morph per second during morphing and rendering. We first obtain the multi-view images along with their corresponding COLMAP camera annotations, and then generate the morphing output using their [open-source code](#) with the default parameter settings.

A.7 Comparisons with Shape Morphing Methods

As shown in Tab. 2, our setting focuses on textured 3D morphing, a task currently shared only with MorphFlow [Tsai et al. 2022].

Earlier works like NeuroMorph [Eisenberger et al. 2021] and CharacterMixer [Zhan et al. 2024] were trained on aligned datasets, essentially learning in-domain, topology-aligned correspondences between 3D data. However, these methods fail to generalize such correspondences to out-of-domain 3D representations. Other methods, such as MeshUp [Kim et al. 2024] and SRIF [Sun et al. 2024], explored shape morphing by leveraging generative priors. While they recognized the importance of generative priors for improving generalization in morphing tasks, their work was limited to shape-only morphing and did not release source code. We qualitatively compared results from their manuscripts with ours, demonstrating that our method not only performs morphing between textured 3D representations with similar topologies (e.g., Mario and Luigi) but also handles morphing between representations with significant category differences (e.g., a boot and a teddy bear).

A.8 Exploratory Experiments with Explicit Correspondence

Inspired by traditional shape morphing and image morphing, our initial method aimed to establish explicit correspondences between textured 3D representations. Specifically, we sought to assign DIFT [Tang et al. 2023] features to each Gaussian [Huang et al. 2024c]. This method was based on the fact that DIFT features have been validated to provide 3D correspondence for the same object from different viewpoints and semantic correspondence across objects, making this introduction reasonable.

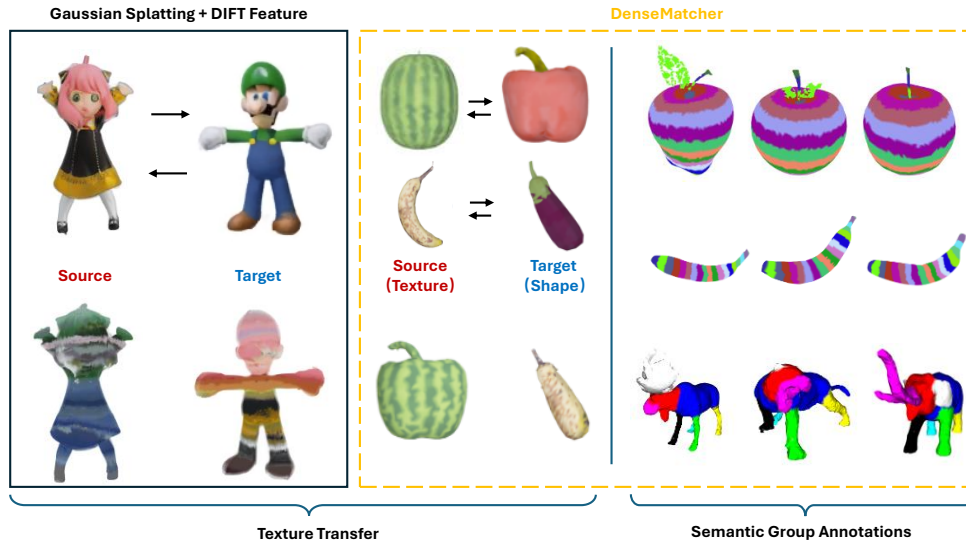


Fig. 13. Exploring possibilities based on explicit correspondence. Using explicit correspondence for morphing presents two major challenges: first, obtaining semantic features for tens of thousands of points is extremely difficult; second, the correspondences obtained are typically part-wise, which is inadequate for morphing tasks that require dense correspondences. Note that the results within the yellow dashed boxes are from DenseMatcher [Zhu et al. 2024] manuscript.

However, we overlooked a key issue: the large number of 3D points, which led to two main drawbacks: (a) high computational cost and (b) the feature handling, which works well for single-point-to-single-point searches from a single viewpoint in 2D foundation models, becomes difficult when attempting to preserve the feature’s approximate consistency across different viewpoints.

After extensive optimization and adjustment of parameters, we obtained a mapping and performed texture transfer between two cartoon characters. We found that the learned correspondence was inaccurate and exhibited a “layered” characteristic, which closely resembled the patterns discovered by DenseMatcher [Zhu et al. 2024]. However, this correspondence is unsuitable for morphing and would require substantial research effort to address. Therefore, we are more inclined to pursue morphing research based on promising 3D generation models with implicit correspondence.

A.9 Testing Protocol and Cases

A.9.1 Quantitative Test Details. For the FID test, the reference images consist of 3000 samples, which were obtained by rendering 15 sets of 3D pairs from 100 different viewpoints. The test images consist of 1500 samples, generated by each method using the same 3D pairs. The remaining quantitative metrics are obtained from testing on the 15 pairs of data.

When evaluating the structural and semantic plausibility of the generated images using GPT-4o, we input the results generated by six methods on the same 3D pairs into GPT-4o for comparison and scoring (similar to the images in Fig. 6). Meanwhile, we provide a guiding prompt that instructs GPT-4o to engage in a step-by-step reasoning process during the evaluation, enhancing both the interpretability and accuracy of the assessment: “What I am doing now is morphing with textured 3D representations, the purpose is to

generate an intermediate interpolation sequence, and at the same time require the transition from source to target to be smooth and reasonable. Now I have six methods, where the first row will give the source and target, and each of the remaining rows is a method. Columns 1-3 are the first test example (morphing from teapot to bowl), columns 4-6 are the second test example (morphing from polar bear to wooden stool), and columns 7-9 are the third test example (morphing from pumpkin to mushroom). Please help me score these methods for the generated intermediate morphing results in terms of shape rationality and semantic rationality, 0 is the lowest score and 1 is the highest score, and give the discrimination results.”

A.9.2 Prompts for Testing Cases. The strength of our method lies in its ability to perform morphing on diverse cross-category or same-category 3D object pairs. This capability was carefully considered during the selection of test cases, which were primarily categorized into furniture, vehicles, plants, humanoid objects, and animals. Moreover, our method goes beyond shape-only morphing, as we also aim to validate its effectiveness on diverse and richly textured color variations. As such, the color range in our test cases is intentionally broad to ensure comprehensive evaluation. More details about the test cases and their corresponding prompts can be found in Tab. 5.

A.10 Raw Statistics of User Study

We recruited over 20 volunteers for a user study, where they were asked to rank morphing sequences generated by six methods for the same pairs of test samples. Presenting the results of different methods simultaneously allows users to clearly observe their differences, making the comparison more fair. The 3D object pairs and results are presented in Tab. 3 and Tab. 4.

	Teapot - Bowl		Polar Bear - Stool		Pumpkin - Mushroom		Teddy Bear - Boot		Mario - Luigi		Average	
	STP-U↑	SEP-U↑	STP-U↑	SEP-U↑	STP-U↑	SEP-U↑	STP-U↑	SEP-U↑	STP-U↑	SEP-U↑	STP-U↑	SEP-U↑
DiffMorpher	0.25	0.20	0.13	0.33	0.60	0.50	0.75	0.40	0.70	0.30	0.49	0.35
AID	0.15	0.53	0.40	0.27	0.50	0.60	0.25	0.32	0.70	0.60	0.40	0.46
MV-Adapter	0.65	0.67	0.07	0.40	0.10	0.50	0.35	0.20	0.02	0.45	0.24	0.44
Luma	0.50	0.13	0.73	0.60	0.10	0.25	0.60	0.60	0.00	0.25	0.39	0.25
MorphFlow	0.45	0.47	0.67	0.53	0.70	0.40	0.30	0.52	0.40	0.40	0.50	0.46
Ours	1.00	1.00	0.40	0.87	1.00	0.75	0.75	0.96	1.00	1.00	0.83	0.92

Table 3. The raw statistics for user study (Part 1).

	Animal Skull - Cow		Car - Truck		House - Church		Chair - Donut		Tank - Cannon		Average	
	STP-U↑	SEP-U↑	STP-U↑	SEP-U↑	STP-U↑	SEP-U↑	STP-U↑	SEP-U↑	STP-U↑	SEP-U↑	STP-U↑	SEP-U↑
DiffMorpher	0.20	0.20	0.36	0.40	0.20	0.25	0.45	0.40	0.70	0.00	0.38	0.25
AID	0.50	0.40	0.28	0.55	0.30	0.65	0.30	0.80	0.40	0.33	0.36	0.55
MV-Adapter	0.20	0.27	0.28	0.40	0.10	0.10	0.45	0.20	0.00	0.33	0.21	0.26
Luma	0.30	0.60	0.52	0.45	0.70	0.35	0.20	0.00	0.50	0.67	0.44	0.41
MorphFlow	0.80	0.53	0.56	0.30	0.70	0.65	0.60	0.60	0.40	0.67	0.61	0.55
Ours	1.00	1.00	1.00	0.90	1.00	1.00	1.00	1.00	1.00	1.00	1.00	0.98

Table 4. The raw statistics for user study (Part 2).

Index	Objects	Prompts
1	Stool	"A wooden tripod stool."
2	Chair	"A blue plastic chair."
3	Llama	"A realistic 3D model of a llama."
4	Dog	"A realistic 3D model of a Husky dog with a big head"
5	Pumpkin	"A flat, orange, pixelated Lego pumpkin with a green stem."
6	Mushroom	"A light green mushroom."
7	Car	"A sleek car with smooth curves, shiny metallic surface, and detailed wheels."
8	Truck	"A large red truck with a spacious cargo bed, sturdy wheels, and a robust front grille."
9	Lounge Sofa	"A purple lounge sofa."
10	Massage Sofa	"A pink medieval-style massage sofa with intricate carvings, plush upholstery, and a comfortable, luxurious design."
11	Mario	"A cartoon-style Mario character with a red hat, blue overalls, white gloves, and a cheerful expression."
12	Luigi	"A cartoon-style Luigi character with a green hat, blue overalls, and a tall, thin build."
13	Tank	"A 3D model of a military tank with detailed textures."
14	Teapot	"A classic teapot."
15	Bowl	"A simple teal bowl."
16	Fighter Jet	"A sleek fighter jet with sharp aerodynamic lines, detailed metallic surface, and camouflage paint."
17	Seagull	"A seagull with detailed wings, a sleek body, and a realistic beak, in natural white and gray colors."
18	Cannon	"A cannon with a long, cylindrical barrel mounted on a wooden carriage."
19	House	"A toy house in a fairy-tale style with whimsical architecture, pastel colors, and charming details like a crooked chimney and flower decorations."
20	Church	"A classic church with tall spires, arched windows, and a large central entrance."
21	Skull	"A 3D model of a human skull."
22	Animal Skull	"A 3D low poly model of an animal skull with gray appearance."
23	Dinosaur	"A dinosaur with a large, muscular body, a long tail, and realistic skin texture."
24	Teddy Bear	"A red teddy bear."
25	Polar Bear	"A low poly model of a polar bear with simplified geometric shapes and flat surfaces, featuring a white body and strong build."
26	Cow	"A simple cow model with a stocky body, short legs, and small horns."
27	Cap	"A blue baseball cap."
28	Helmet	"A medieval helmet with a rounded metal shell and a faceplate."
29	Donut	"A donut with a round shape, a hole in the center, and a sugary glaze."
30	Ice Cream	"Pink ice cream with a creamy texture, served in a cone or cup."
31	Hydrant	"A fire hydrant with a cylindrical body, typically painted in bright red."
32	Drum	"A metal oil drum with a cylindrical shape, a top and bottom lid, and a rugged surface."
33	Vase	"A light purple vase."
34	Boot	"A snow boot with a thick, insulated lining, waterproof exterior, and durable sole for winter conditions."
35	Fish	"A chubby fish with a vibrant green body."

Table 5. Prompts for testing cases.